



THIS MANUSCRIPT HAS BEEN SUBMITTED TO THE JOURNAL OF GLACIOLOGY AND HAS NOT BEEN PEER-REVIEWED.

Ice Surface Change Drives Subglacial Hydrologic Reorganization and Interior Speedup in Northwest Greenland

Journal:	<i>Journal of Glaciology</i>
Manuscript ID	Draft
Manuscript Type:	Article
Date Submitted by the Author:	n/a
Complete List of Authors:	Sommers, Aleah; Dartmouth College, Thayer School of Engineering Stubblefield, Aaron; University of Maryland; NASA Goddard Space Flight Center Andrews, Lauren; NASA Goddard Space Flight Center, Cryospheric Sciences Laboratory Meyer, Colin; Dartmouth College, Thayer School of Engineering Smith, Benjamin; University of Washington,
Keywords:	Subglacial processes, Laser altimetry, Ice-sheet modelling, Glacier hydrology, Arctic glaciology
Abstract:	Changes in ice surface elevation and slope influence subglacial water pressure and sliding velocity. Leveraging decadal scale changes in elevation observed by the Ice, Cloud, and land-Elevation satellite (ICESat) and ICESat-2 missions, we use coupled subglacial hydrology--ice dynamics modeling applied to a section of the northwest Greenland Ice Sheet to explore i) how decadal scale changes in ice surface elevation influence changes in winter background state subglacial hydrology and corresponding ice velocity, and ii) how much glacier seasonal response is attributable to geometry compared to environmental forcing. Our simulations suggest a complex reorganization of the subglacial hydrologic system between 2004 and 2020, as a result of changes in surface elevation, which drives the redistribution of freshwater flux between fjords, an overall acceleration trend in the interior, and an increase in

	<p>background basal melt. We also find that the winter background state of the subglacial system modulates the seasonal response. This demonstrates a potential feedback that exacerbates mass loss from the Greenland Ice Sheet as surface elevation evolves, while also highlighting the subtleties involved in accounting for changes in effective pressure, ice velocity, and basal melt due to changes in subglacial hydrology.</p>

SCHOLARONE™
Manuscripts

Ice Surface Change Drives Subglacial Hydrologic Reorganization and Interior Speedup in Northwest Greenland

Aleah N. SOMMERS,¹ Aaron STUBBLEFIELD,^{2,3} Lauren ANDREWS,³ Colin R. MEYER,¹
Benjamin E. SMITH⁴

¹*Thayer School of Engineering, Dartmouth College, Hanover, NH, USA*

²*University of Maryland, College Park, MD, USA*

³*NASA Goddard Space Flight Center, Greenbelt, MD, USA*

⁴*Applied Physics Laboratory, University of Washington, Seattle, WA, USA*

Correspondence: Aleah Sommers <aleah.n.sommers@dartmouth.edu>

ABSTRACT. Changes in ice surface elevation and slope influence subglacial water pressure and sliding velocity. Leveraging decadal scale changes in elevation observed by the Ice, Cloud, and land-Elevation satellite (ICESat) and ICESat-2 missions, we use coupled subglacial hydrology–ice dynamics modeling applied to a section of the northwest Greenland Ice Sheet to explore i) how decadal scale changes in ice surface elevation influence changes in winter background state subglacial hydrology and corresponding ice velocity, and ii) how much glacier seasonal response is attributable to geometry compared to environmental forcing. Our simulations suggest a complex reorganization of the subglacial hydrologic system between 2004 and 2020, as a result of changes in surface elevation, which drives the redistribution of freshwater flux between fjords, an overall acceleration trend in the interior, and an increase in background basal melt. We also find that the winter background state of the subglacial system modulates the seasonal response. This demonstrates a potential feedback that exacerbates mass loss from the Greenland Ice Sheet as surface elevation evolves, while also highlighting the subtleties involved in accounting for changes in effective pressure, ice velocity, and basal melt due

28 **to changes in subglacial hydrology.**

29 INTRODUCTION

30 The Greenland Ice Sheet is a prominent frozen reservoir of freshwater on Earth. In recent decades, it has
31 had a negative mass balance, losing more ice through melt, runoff, and iceberg calving than it gains each
32 year through snow accumulation that gradually compacts into ice (Mouginot and others, 2019; Mankoff and
33 others, 2020). Although widespread satellite observations in recent years have improved the monitoring of
34 overall mass loss of the Greenland Ice Sheet (Shepherd and others, 2012; Hanna and others, 2013; Mouginot
35 and others, 2019; Smith and others, 2019), gaps remain in scientific understanding of the physical processes
36 governing dynamics of the ice sheet and how these will impact mass loss in the future. A particular source of
37 uncertainty in future sea level projections associated with ice mass loss is the role of subglacial hydrology, or
38 liquid water at the interface between the ice and the underlying bed material. The subglacial environment
39 is difficult to access for direct observations, but numerical models can provide insights into basal processes
40 by simulating the relevant physical processes of water and ice flow, melt, and sliding.

41 Subglacial hydrology affects the velocity of glaciers by modulating how easily the ice slides over its
42 bed. Glacier sliding parameterizations (or “sliding laws”) are generally formulated in terms of basal stress,
43 calculated as a function of ice sliding velocity and effective pressure, which is defined as the difference
44 between ice overburden pressure and water pressure at the bed (Budd and others, 1979; Schoof, 2005).
45 The specific relationship and exponents vary between different sliding laws, but sliding velocity and effective
46 pressure typically have a nonlinear relationship.

47 Water below glaciers flows according to pressure gradients, which are partly determined by geomet-
48 ric properties of the glacier, such as surface slope, ice thickness, and bed slope, and partly by fluid flow
49 dynamics. Pressure evolves dynamically through space and time with evolving glacier geometry and hy-
50 draulic processes. Water moves from high to low pressure, meaning that in some cases water can flow
51 uphill relative to the bed or surface topography. Although bed topography beneath the ice is difficult to
52 accurately constrain, ice surface elevation has been relatively well observed since 2003 with NASA’s Ice,
53 Cloud and land-Elevation satellite (ICESat) and follow-up Operation IceBridge (MacGregor and others,
54 2021) and ICESat-2 laser altimetry missions, by which the travel time of laser pulses is used to measure
55 the elevation of Earth’s surface (Schutz and others, 2005; Abdalati and others, 2010; Markus and others,

56 2017). Changes in ice surface elevation and surface slope cause changes in the hydraulic pressure gradient
57 at the bed.

58 Liquid water beneath glaciers is derived from melting at the base of the ice as well as seasonal surface
59 melting that drains through the ice. During the winter months, the subglacial system receives water primar-
60 ily from basal melt and is in a relatively stable background state. During the summer months, a significant
61 fraction of the water that melts on the surface of the ice sheet drains to the bed via moulins and crevasses
62 (Meierbachtol and others, 2013; Andrews and others, 2014; Smith and others, 2015). At higher elevations,
63 a portion of surface melt percolates into porous firn and refreezes instead of running off (Meyer and Hewitt,
64 2017; Rennermalm and others, 2022). Intuitively, one might expect that more meltwater being produced
65 on the ice sheet would lead to more water at the bed, and a corresponding increase in water pressure and
66 acceleration. However, this is not necessarily the case – as has been observed through field observations
67 and represented in numerical models (Schoof, 2010; Flowers, 2015) – with sufficient meltwater inputs to
68 the bed, the drainage system will transition to form an efficient system of channelized pathways. These
69 efficient conduits decrease water pressure and consequently pull water from the surrounding bed, increasing
70 friction and yielding a deceleration even with increasing melt (Sundal and others, 2011). This negative
71 feedback complicates predicting future development of Greenland glacier seasonal velocities, and numerous
72 scientific studies have attempted to understand when and where such channelized drainage is likely to
73 develop (Banwell and others, 2016; Cowton and others, 2016; Simkins and others, 2021; Rada Giacaman
74 and Schoof, 2023; Warburton and others, 2024).

75 In this study, we are motivated by questions that address the impact of the background state and
76 seasonal evolution of the subglacial system: 1) How do decadal scale changes in surface elevation influence
77 changes in winter background state subglacial hydrology and corresponding ice dynamics of the Greenland
78 Ice Sheet? 2) How much is seasonal velocity attributable to glacier geometry compared to environmental
79 forcing? Leveraging ice surface elevation derived from ICESat and ICESat-2 observations, we use a coupled
80 subglacial hydrology–ice dynamics model to simulate changes in effective pressure and ice velocity over the
81 period 2004 to 2020.

82 In the following sections, we describe our methods, including how we generate our high-resolution
83 DEMs, the models and data we use, and our experimental approach. We then present simulation results
84 and discuss implications of our findings.

85 METHODS

86 DEM generation

87 We generate high-resolution DEMs of the Greenland Ice-Sheet surface based on a combination of ICESat
88 and ICESat-2 satellite laser altimetry, Operation IceBridge airborne laser-altimetry data, and ArcticDEM
89 digital elevation models. We combine these using a surface-fitting algorithm adapted from the algorithm
90 developed for the ICESat-2 ATL14 and ATL15 gridded height and height-change data products, with
91 additional processing steps added to help correct for potential artifacts in the other datasets. The ATL14/15
92 algorithm (Smith and others, 2025; Smith, 2025) approximates ice-sheet elevations as the sum of a fine-
93 resolution reference DEM and a set of coarser-resolution elevation-change surfaces. For example, the ICESat-2
94 project generates a 100-m DEM (ATL14) and a set of elevation-change surfaces with 1 km horizontal and
95 0.25 yr temporal resolution. The algorithm works by minimizing a functional that depends on the roughness
96 of the DEM, the roughness of the elevation-change rate described by the elevation-change surfaces, and the
97 uncertainty-scaled misfit between the estimated elevation (equal to the sum of the DEM and the elevation-
98 change surfaces) and the ICESat-2 data points. The combined ATL14 and ATL15 data products give well
99 constrained estimates of surface height during the ICESat-2 mission (2019-2025) along reference ground
100 tracks that ICESat-2 has measured repeatedly, but the accuracy of the surface-height estimates declines in
101 the gaps between these tracks (Smith and others, 2025). We use a modified version of this algorithm with
102 an extended set of input data products to generate a set of high-resolution DEMs spanning 2004-2020.

103 Our DEM generation is carried out in two stages. In the first stage, we apply the surface-fitting
104 algorithm to a combination of ICESat-2 and ArcticDEM data to generate a high-resolution (50 m) DEM
105 referenced to decimal year 2020.5. In the second stage, we subtract this DEM from a multi-decadal time
106 series of ICESat and IceBridge laser-altimetry data to produce a set of elevation-difference measurements
107 spanning 2004-2020. We then apply the surface-fitting algorithm to these difference measurements to
108 produce a time series of gridded elevation differences with 500 m horizontal and 1 yr temporal node
109 spacing. See the Supplemental Information for more details.

110 Model description

111 To simulate subglacial hydrology, we use the Subglacial Hydrology And Kinetic, Transient Interactions
112 model (SHAKTI; Sommers and others (2018)) coupled with ice dynamics in the Ice-sheet and Sea-level

113 System Model (ISSM; Larour and others (2012)). SHAKTI is a physics-based model that calculates
114 evolving hydraulic head, effective pressure, subglacial gap height, water flux, and basal melt. The model
115 internally calculates spatiotemporally variable hydraulic transmissivity, allowing for turbulent, laminar, and
116 transitional flow regimes to develop, and flexible drainage geometries to emerge that represent a continuum
117 from inefficient/distributed drainage, to efficient/channelized drainage. ISSM is a state-of-the-art glacier
118 ice flow model that uses finite element methods on adaptable meshes to simulate a variety of processes that
119 impact ice dynamics. SHAKTI is built into ISSM as a module to facilitate coupling between subglacial
120 hydrology and ice velocity, which occurs through the friction parameterization, or sliding law, in which
121 basal stress depends on both effective pressure (calculated by SHAKTI) and ice sliding velocity (calculated
122 by the stress balance in ISSM). We use the same form of the SHAKTI equations as in Sommers and others
123 (2024). The simulations presented in this paper use the Budd-type sliding law (Budd and others, 1979)
124 and the Shallow Shelf Approximation (MacAyeal, 1989) for ice flow. See Table S1 for a list of parameter
125 values.

126 Our model domain is a region in Northwest Greenland (Fig. 2a), selected as a focus area because of its
127 significant change in surface elevation and numerous fjords with outlet glaciers. The finite element mesh
128 consists of 129,273 triangular elements, using adapted resolution based on observed surface velocity, with
129 element edge lengths ranging from 100 m to 20 km. We use ice thickness and bed elevation estimates from
130 BedMachine v5 (Morlighem and others, 2021). After prescribing the 2004 ice geometry for our domain, we
131 perform an inversion to infer a spatially variable friction coefficient used in the sliding law (Sommers and
132 others, 2024). In standard practice ice sheet modeling, this friction coefficient is typically used to represent
133 the lumped influence of variable conditions at the bed, including variations in effective pressure. Because
134 we explicitly account for spatial and temporal variations in effective pressure in our coupled hydrology
135 simulations, here the friction coefficient primarily represents bed material properties that influence basal
136 friction and presumably remains relatively unchanged over the decadal time scales considered here. We
137 hold this friction coefficient consistent in all our simulations, but the basal stress evolves with changes in
138 effective pressure. This is in contrast to the transient calibration approach of Badgeley and others (2025),
139 for example, in which sequential inversions are performed to infer a friction coefficient, while assuming a
140 static effective pressure distribution.

141 *Winter background hydrology and velocity*

142 We run coupled SHAKTI-ISSM spin-up simulations for one year to generate the winter “background state”
143 hydrology and velocity conditions for snapshots at 2004, 2008, 2012, 2016, and 2020. Ice geometry remains
144 unchanged during each simulation, with surface elevation set by the DEM for each year. In these winter
145 simulations, we assume that all meltwater present in the subglacial system is produced by basal melt
146 through a combination of geothermal flux, frictional heat from sliding, and turbulent dissipation. The
147 winter background sets the initial conditions for the melt season in Greenland, with some amount of
148 drainage structure sustained below the ice. Far from being stagnant, active subglacial hydrological systems
149 persist through the winter, supplied by basal melt (Sommers and others, 2023).

150 *Seasonal simulations*

151 Beginning from our winter background state simulations for 2004 and 2020, we run transient seasonal
152 simulations using ice sheet surface runoff derived from the MERRA-2 climate reanalysis (Gelaro and
153 others, 2017) to prescribe the magnitude, timing, and distribution of meltwater inputs to the bed. We
154 direct all surface runoff immediately to the bed at the location where the water is produced, neglecting
155 the nuances of routing, refreezing, or storage in the supraglacial and englacial drainage systems. In order
156 to uniquely assess the role of surface geometry in determining hydrological and ice flow under comparable
157 environmental forcing, we force these transient simulations on 2004 and 2020 geometries using the same
158 seasonal runoff data from the mean climatology over the period 2003-2022.

159 **Ice velocity comparison to observations**

160 In order to assess the impact of surface elevation change on ice velocity patterns relative to observations,
161 we compare the modeled winter background states to winter time SAR derived ice velocities (Joughin and
162 others, 2010, 2015, 2018; Joughian, 2023). To complete this analysis, we use observations dated from 2000
163 to 2020; 2000 is used because the next image is from 2005/2006. Table S2 presents a list of the specific
164 images used. Velocity images span variable ranges, but do not include the summer melt season (June, July
165 and August). We then calculate the linear velocity trend of each pixel. Using the linear trend, we determine
166 the expected velocity at the model time steps of 2004.5 and 2020.5. We perform the same analysis for
167 the winter background model outputs after regridding the model outputs to the observational grid of 500
168 m x 500 m. This processing permits us to directly compare the observations and model outputs while

169 minimizing the impact of interannual variability.

170 **MODEL RESULTS**

171 Figure 1 presents ice surface velocity, subglacial water flux, and effective pressure modeled using 2004 and
172 2020 surface elevations. Modeled velocity, water flux, and effective pressure all vary spatially, and overall
173 display the same large-scale structure in both years. The differences between the two, however, reveal
174 notable changes attributable to changes in surface elevation. These changes are discussed next.

175 *Ice surface elevation changes*

176 Figure 2a shows the difference in ice surface elevation (2020 - 2004) over the Greenland Ice Sheet as observed
177 by the ICESat and ICESat-2 missions, based on the DEMs described above. Significant elevation decrease
178 (i.e. ice sheet thinning) is visible around the margins of the ice sheet, and no significant increase in surface
179 elevation is apparent. Some major outlet glaciers show large areas of pronounced surface lowering in excess
180 of 100 m over this period, with widespread thinning along the northwest coast. Incremental changes every
181 four years over this period are presented in Figs. S1 and S2, with a general pattern of steady thinning
182 around the ice sheet margins over each segment of time.

183 *Changes in winter water flux, effective pressure, velocity, and basal melt*

184 Figure 2b-g present spatial plots of modeled changes in winter subglacial water flux, effective pressure, ice
185 velocity, and basal melt rate as simulated by the coupled model SHAKTI-ISSM for the ICESat (2004) and
186 ICESat-2 (2020) eras in northwest Greenland, with changes plotted as the difference between these results
187 (2020 minus 2004). Incremental changes every four years over this period are presented in Figs. S2-S5.
188 Changes in subglacial water flow paths caused by changes in surface elevation are clearly visible as blue
189 and red pathways in Fig. 2b. Red indicates a decrease in winter water flux and blue indicates an increase
190 in winter water flux over the period 2004 to 2020. The difference between 2020 and 2004 shows a mix of
191 increases and decreases in water flux at different places. Incremental four-year simulation steps suggest that
192 background water flux generally increased in the interior from 2004 to 2008 with some notable switches in
193 subglacial water flow paths, further reorganized between 2008-2012 and 2012-2016, and experienced more
194 of an overall decrease from 2016-2020 (Fig. S2), resulting in the full mixed reconfiguration apparent in Fig.
195 2b. For a closer view of the redirection of water flux, percent change in modeled subglacial water flux is

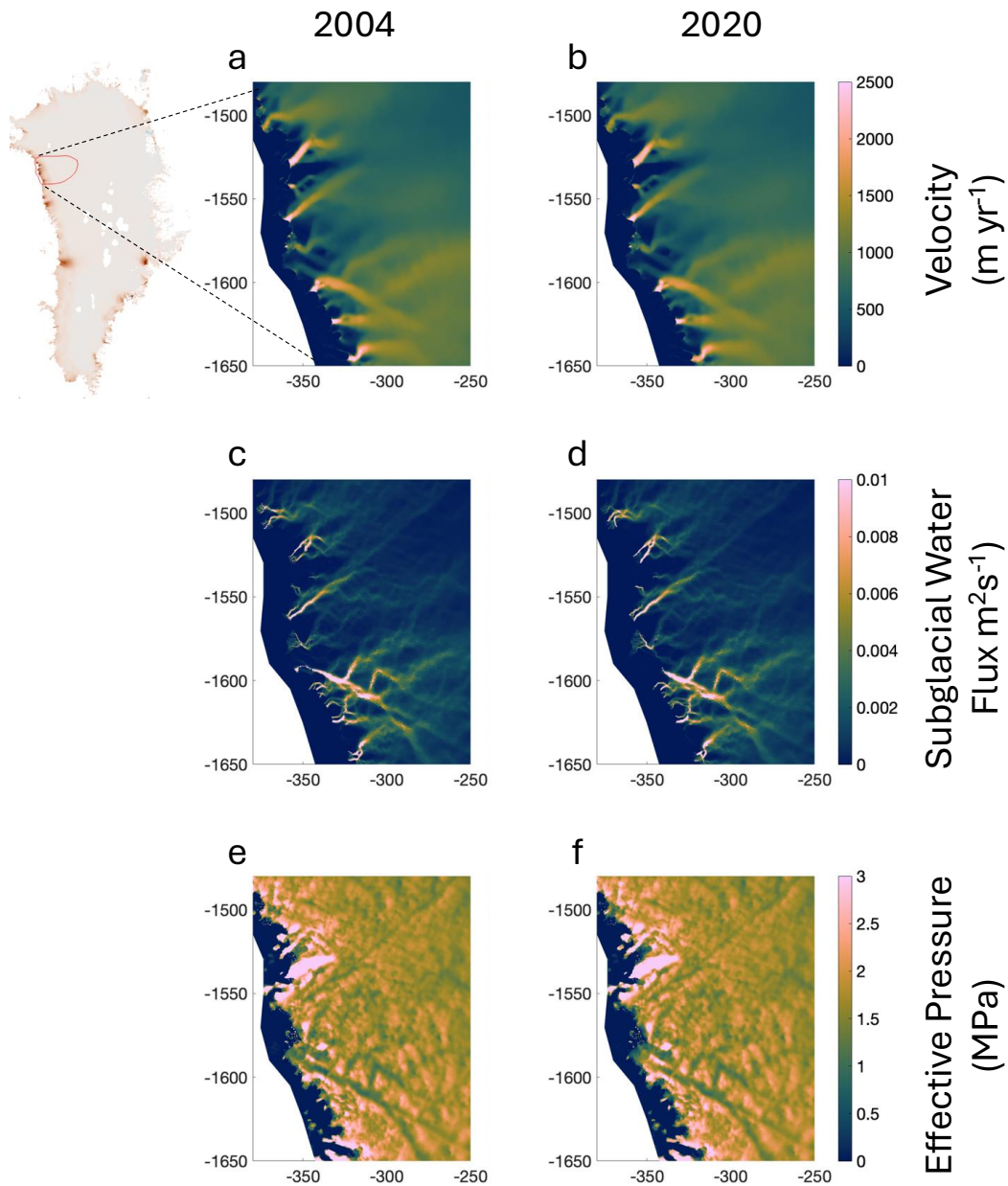


Fig. 1. Model domain in NW Greenland and modeled ice velocity in 2004 (a) and 2020 (b). Modeled subglacial water flux in 2004 (c) and 2020 (d). Modeled effective pressure in 2004 (e) and 2020 (f). All x and y axes are in polar stereographic projection (EPSG: 3413) with units of km.

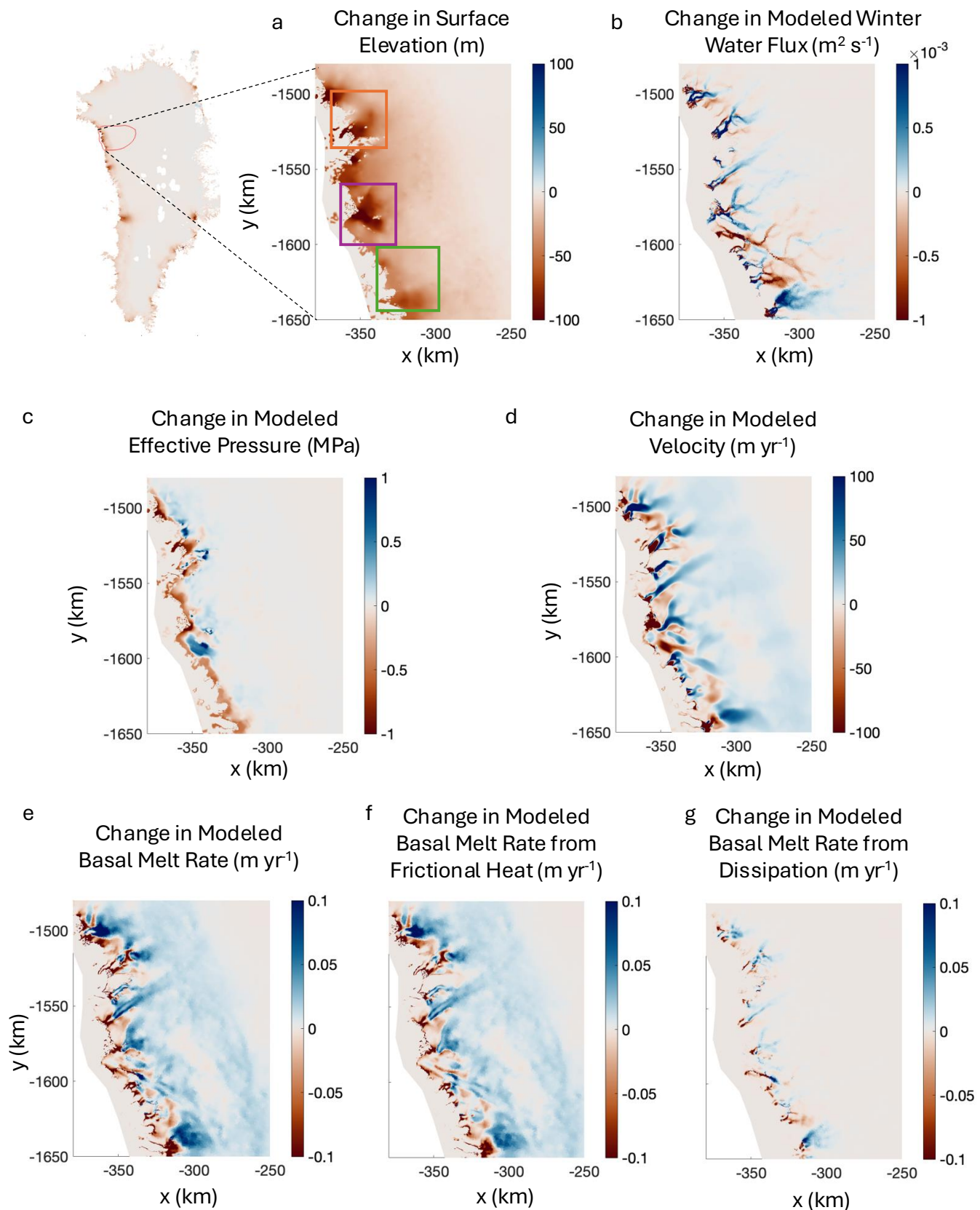


Fig. 2. a) Change in ice surface elevation between 2004 and 2020 over the Greenland Ice Sheet, with model domain in NW Greenland. b-d) Modeled change in background state subglacial water flux (b), effective pressure (c), and ice velocity (d) between 2004 and 2020. e-g) Modeled change in total basal melt rate (e) and change in basal melt rate due to frictional heat (f) and dissipation (g).

196 shown in Fig. 3a,d, and g for three selected areas.

197 Modeled effective pressure reveals a consistent decrease in effective pressure near the margin (red),
198 with a general increase in effective pressure in the interior (Fig. 2c). A closer look is provided into percent
199 change in modeled effective pressure in Fig. 3b, e, and h. These changes, however, do not develop through
200 a linear progression, as seen in the four-year incremental change plots in Fig. S3, but rather exhibit more
201 widespread changes in effective pressure during the 2004-2008 and 2016-2020 periods, with relative stability
202 during 2008-2012 and 2012-2016, except for localized increases in effective pressure.

203 Simulated velocities show deceleration in some outlet glaciers near the margin, while others accelerate,
204 and overall a dominating acceleration trend further inland over the full period 2004 to 2020 (Fig. 2d), with
205 a zoomed in perspective for detail of percent change in velocity in Fig. 3c, f, and i. When viewed over
206 four-year increments, again these patterns of change do not develop linearly over time, but instead show up
207 with mixed acceleration and deceleration during 2004-2008 (Fig. S4). From 2008-2012 and 2012-2016, the
208 modeled velocity change continues to be mixed, with areas of acceleration and deceleration. The period
209 2016-2020 shows a broad pattern of mild deceleration in the interior with pronounced acceleration in several
210 outlet glaciers.

211 As calculated by SHAKTI, our simulations suggest a variety of changes in basal melt rate (Fig. 2e)
212 between 2004 and 2020, with locations near the margin experiencing reduced basal melting, and a clear in-
213 crease in basal melt inland. The bulk of the change in basal melt rate is attributable to changes in frictional
214 heat associated with changes in sliding velocity (Fig. 2f). However, turbulent dissipation corresponding to
215 changes in subglacial water flux is significant at some outlet glaciers, leading to increased basal melt from
216 dissipation in places where winter water flux increased or was redirected (Fig. 2g).

217 Through examination of changes in ice velocity, effective pressure, basal melt rate, and subglacial
218 water flux as related to changes in ice surface elevation (Fig. 4), a trend emerges relating a decrease in
219 modeled effective pressure with a decrease in surface elevation (Fig. 4b). However, the relationship is
220 weak for predicting changes in modeled velocity or basal melt rate based on changes in surface elevation
221 (Fig. 4a,c,d). An overall relationship between increasing ice velocity and increasing effective pressure is
222 demonstrated (Fig. 4e). The modeled data, however, display a high degree of variability and generally
223 suggest a lack of predictability of ice velocity response to projected ice thinning. Coupled simulations such
224 as these provide a window into the nonlinear and complicated behavior of ice sheet dynamics.

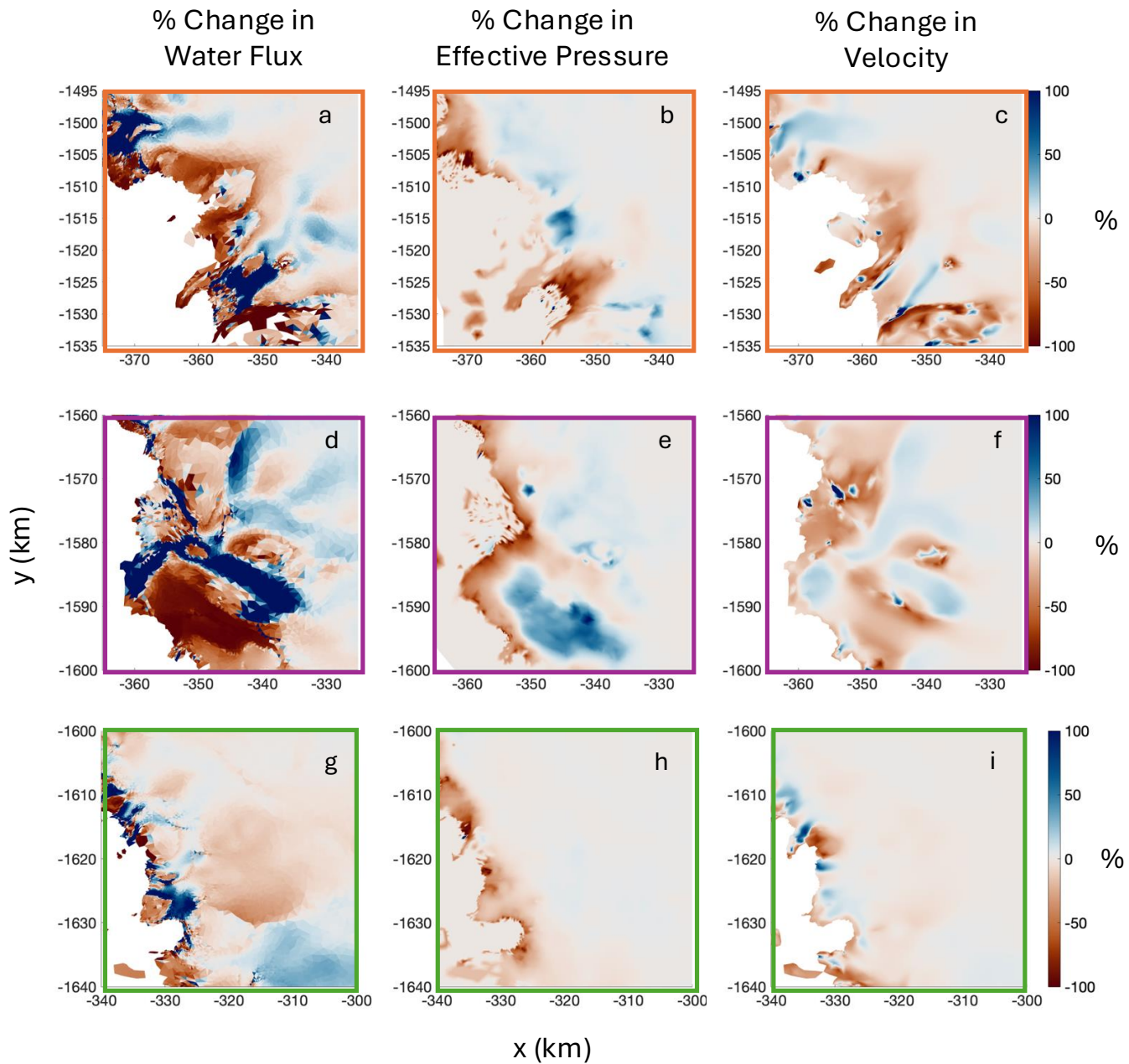


Fig. 3. a) Percent change in modeled background subglacial water flux (a,d,g), effective pressure (b,e,h), and ice velocity (c,f,i) between ICESat (2004) and ICESat-2 (2020) eras, zoomed in for detail in three areas shown on Fig. 2a.

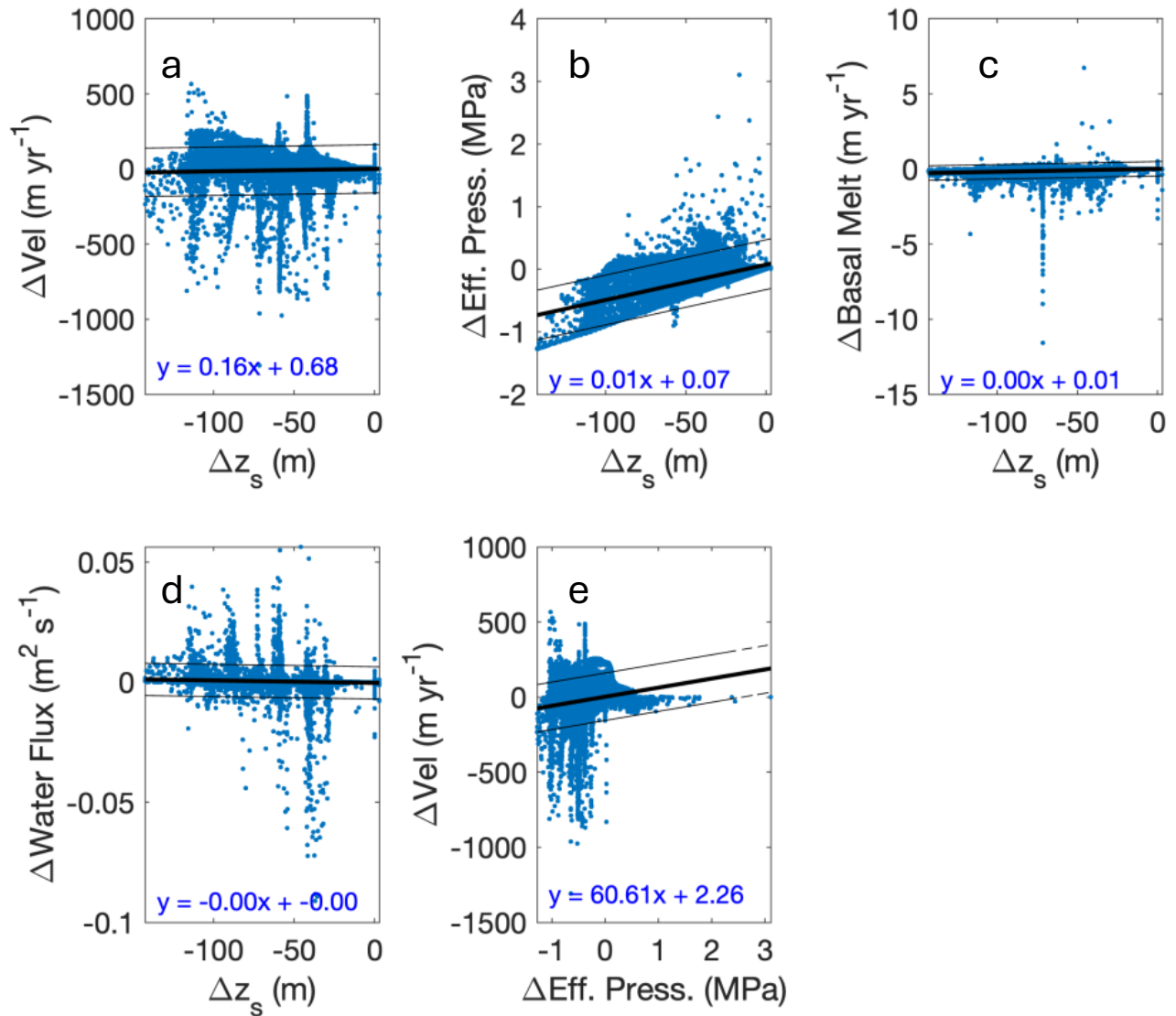


Fig. 4. Change in ice velocity (a), change in effective pressure (b), change in basal melt rate (c), and change in subglacial water flux (d) as a function of change in ice surface elevation. Change in velocity as a function of change in effective pressure (e). Solid dark lines show a linear fit, with $\pm 95\%$ confidence plotted in light dashed lines.

225 **Response to seasonal melt**

226 Figure 5 presents time series of mean modeled effective pressure, subglacial water flux, ice velocity, and
227 total basal melt over our model domain in response to seasonal meltwater forcing based on mean 2003-
228 2022 climatology derived from MERRA-2 reanalysis as described above. For both the 2004 and 2020
229 geometries, subglacial water flux increases during the melt season in response to the runoff inputs, generally
230 corresponding to an increase in velocity and decrease in effective pressure early in the melt season, followed
231 by deceleration and increase in effective pressure following the peak of the melt season at Day 200, and
232 notably an abrupt acceleration near the end of the melt season that corresponds with a decrease in effective
233 pressure as the drainage system shuts down and becomes less efficient. Overall, the shape of the response
234 is similar in both simulations, but with an offset in effective pressure and velocity between the background
235 winter state for the two eras, reflecting a general decrease in both effective pressure and ice velocity in
236 2020 as compared to 2004, simply due to the differences in ice surface elevation. While the response is
237 qualitatively similar, the difference between the two seasonal simulations (2020 minus 2004; Fig. 5d-f)
238 reveals some variation around the background offset, with a slightly less negative response in effective
239 pressure during the peak melt season in 2020 compared with 2004, a slightly more negative response in
240 water flux, and a slightly less negative response in velocity. The relationship between the mean modeled
241 quantities in these seasonal simulations using the 2004 and 2020 geometries are plotted in Fig. 5g-i,
242 showing a near-linear pattern, but with some variation around that. These results show that changes in ice
243 geometry and the background subglacial drainage state influence the seasonal response in coupled behavior
244 of the Greenland Ice Sheet, again highlighting the complex response of the ice sheet to changes in surface
245 elevation.

246 **DISCUSSION**

247 **Changes in subglacial flow paths**

248 Our simulation results show an increase in subglacial water being routed toward areas that have experienced
249 enhanced thinning (i.e. lower surface elevation), drawing water away from outlets that have maintained
250 relatively more of their thickness (Fig. 2b), although this relationship between change in water flux and
251 change in surface elevation is relatively weak when considered over the entire model domain (Fig. 4d). Local
252 changes in subglacial flow paths not only influence ice sliding velocity by changing the pressure distribution

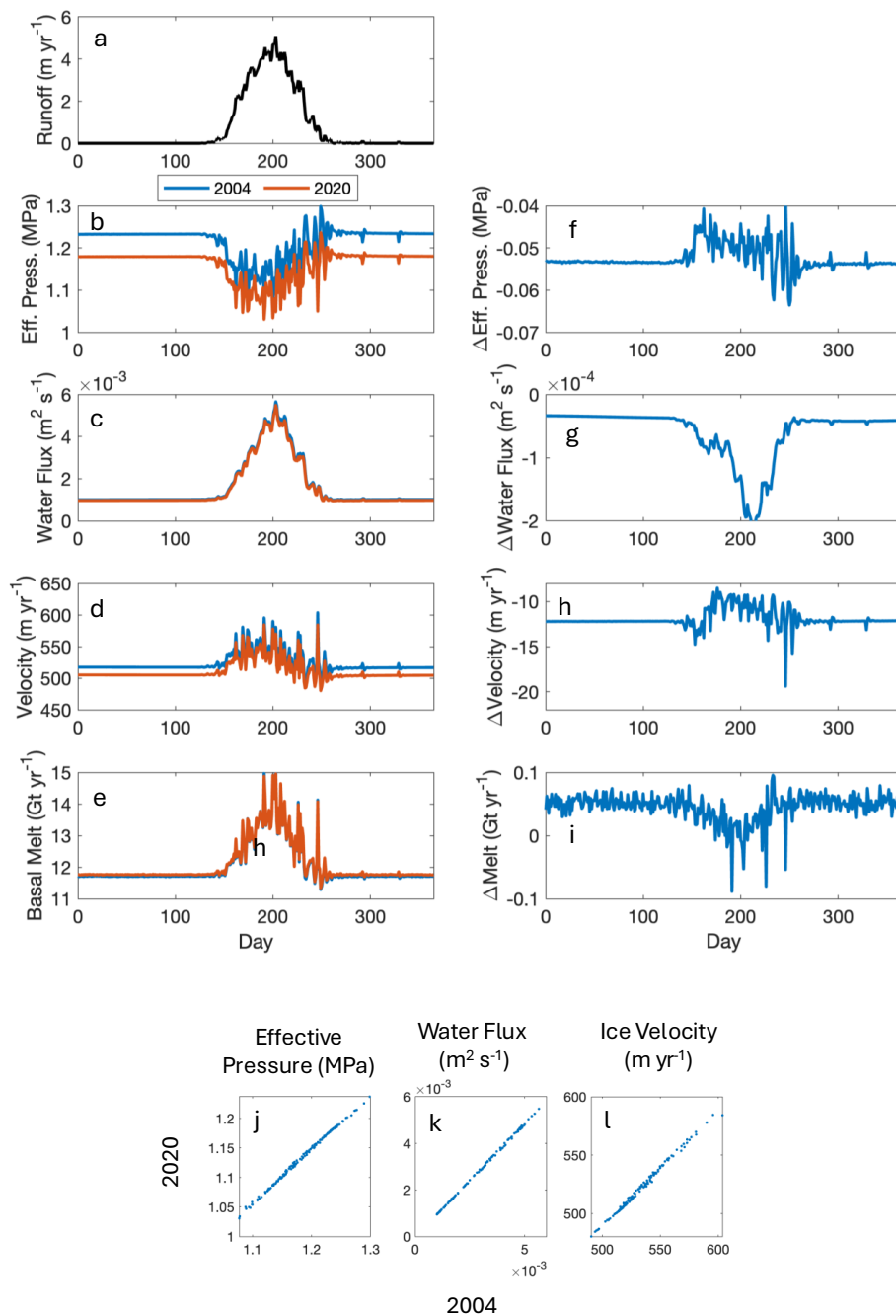


Fig. 5. Mean runoff forcing from 2003-2022 mean MERRA-2 climatology (a), mean modeled effective pressure (b), subglacial water flux (c), ice velocity (d), and total basal melt (e) in response to seasonal meltwater forcing with ice geometry corresponding to the ICESat era (2004; blue) and ICESat-2 era (2020; red). Difference (2020 minus 2004) in mean effective pressure (f), mean subglacial water flux (g), mean ice velocity (h), and total basal melt (i). Relationship of mean effective pressure (j), water flux (k), and velocity (l) between 2004 and 2020 simulations.

253 at the bed, but also hold ramifications for freshwater discharge into fjords. Changes in freshwater flux
254 between neighboring fjords may have wide-ranging impacts such as changes in fjord circulation patterns,
255 biochemistry, frontal melt rates, and terminus position (Straneo and Cenedese, 2015; Jackson and Straneo,
256 2016; Sejr and others, 2022; Vries and others, 2025).

257 **Interior acceleration**

258 We simulate a general decrease in effective pressure near the ice sheet margins, but a modest increase in
259 effective pressure further inland, which corresponds to an overall accelerating trend in simulated winter ice
260 velocity between 2004 and 2020 (Fig. 2c,d). This result may initially seem surprising. If basal conditions
261 remained the same in terms of water pressure, a decrease in ice thickness would lead to a decrease in
262 effective pressure and corresponding acceleration. Our simulations demonstrate a more mixed response.
263 Changes in surface gradients facilitate a reorganization of pressure gradients at the bed that drive the
264 reconfiguration of subglacial water flow and corresponding changes in pressure. These various factors play
265 out in different ways under different specific conditions, and it is worth noting the widespread interior
266 acceleration that occurs even with deceleration in certain locations near the ice sheet margin.

267 **Comparison to velocity observations**

268 We compare our modeled changes in velocity to observed changes in velocity using winter observations
269 derived from synthetic aperture radar (SAR) over the same period. Figure 6 shows the calculated rate of
270 change per year in modeled and observed velocities, and the number of available velocity observations at
271 each location. In general, the model and observations show the same general pattern, with the exception of
272 the very near terminus regions. However, the magnitude of the rate of change is lower in the model than in
273 the observational dataset. Figure 7 shows the percent change in velocity averaged per year over the period
274 between 2020 and 2004, as modeled and observed, and the difference between them. The annual trend
275 in mean modeled and observed velocity is presented in Fig. 8, showing a general acceleration. Overall,
276 modeled velocity changes reproduce the correct spatial patterns, but the magnitude of change between 2020
277 and 2004 is only a fraction of the observed change in velocity. Our winter background modeling approach
278 accounts for changes in surface elevation and changes in subglacial hydrology, isolating these influences from
279 other sources of influence at the terminus such as changes in warm water circulation, changes in terminus
280 position and buttressing support, and other ice/ocean interactions, along with changes in seasonal surface

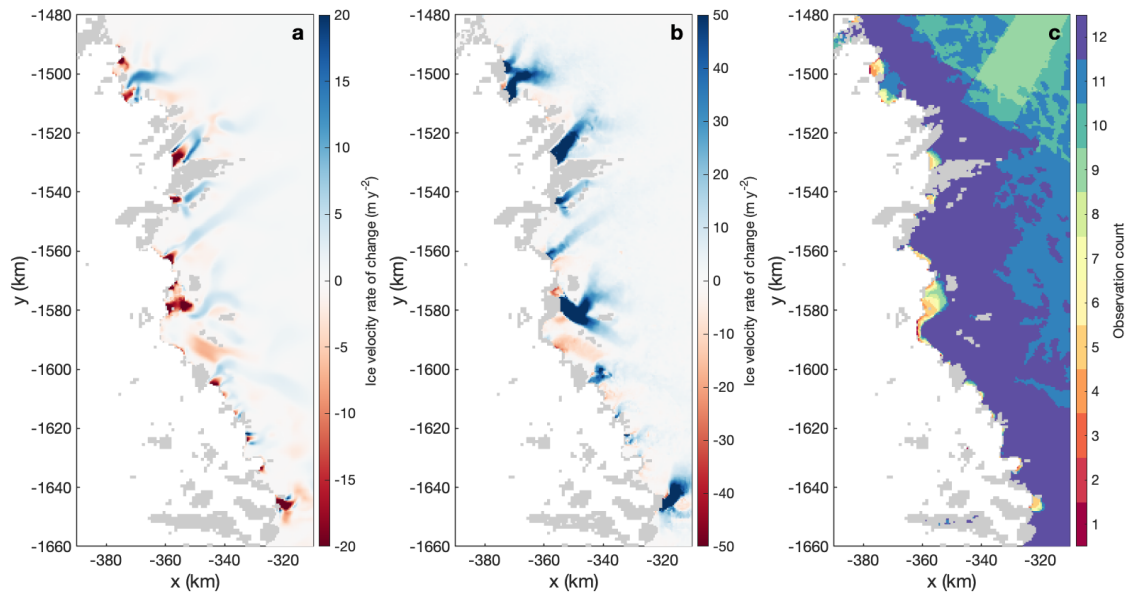


Fig. 6. Rate of change in velocity (2020-2004) as modeled due to change in surface elevation and hydrologic effects (a). Rate of change in observed velocity (b). Count of observations (c).

281 melt. The fact that the model produces velocity changes that generally agree spatially with observations
 282 is encouraging, and we interpret this to represent the magnitude of velocity change that can be attributed
 283 to changes in ice surface elevation and corresponding changes in the subglacial hydrological system.

284 Basal melt changes

285 Ice-sheet mass balance is estimated from melting at the surface, but the ice also melts from below at the
 286 ice-bed interface. The role of basal melting has recently been highlighted as an important consideration for
 287 overall ice-sheet mass balance (Karlsson and others, 2021; Young and others, 2022), although it is difficult
 288 to observe directly and constrain over large time and space scales. SHAKTI calculates total basal melt rate,
 289 along with its components (geothermal, frictional, and turbulent heat), providing an informed estimate of
 290 evolving basal melt. As shown in Fig. 2, changes in ice elevation yield heterogeneous changes in basal
 291 melt rate in the coupled SHAKTI-ISSM model. In the interior, these changes are dominated by changes
 292 in frictional heat, whereas changes in dissipation are important at the outlets, especially in places where
 293 subglacial water flux has increased or decreased through hydrologic reorganization as a result of changes
 294 in surface elevation.

295 Our coupled winter simulations calculate a total background basal melt volume over our model domain

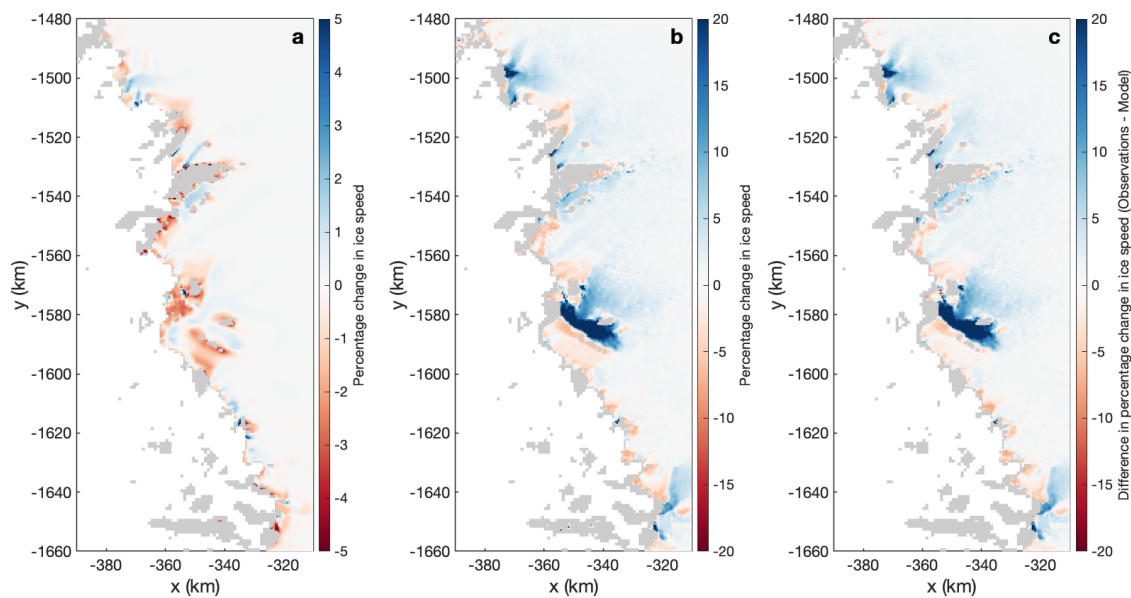


Fig. 7. Percent change in velocity per year as modeled due to change in surface elevation and hydrologic effects (a). Percent change per year in observed velocity (b). Difference between observed and modeled (c).

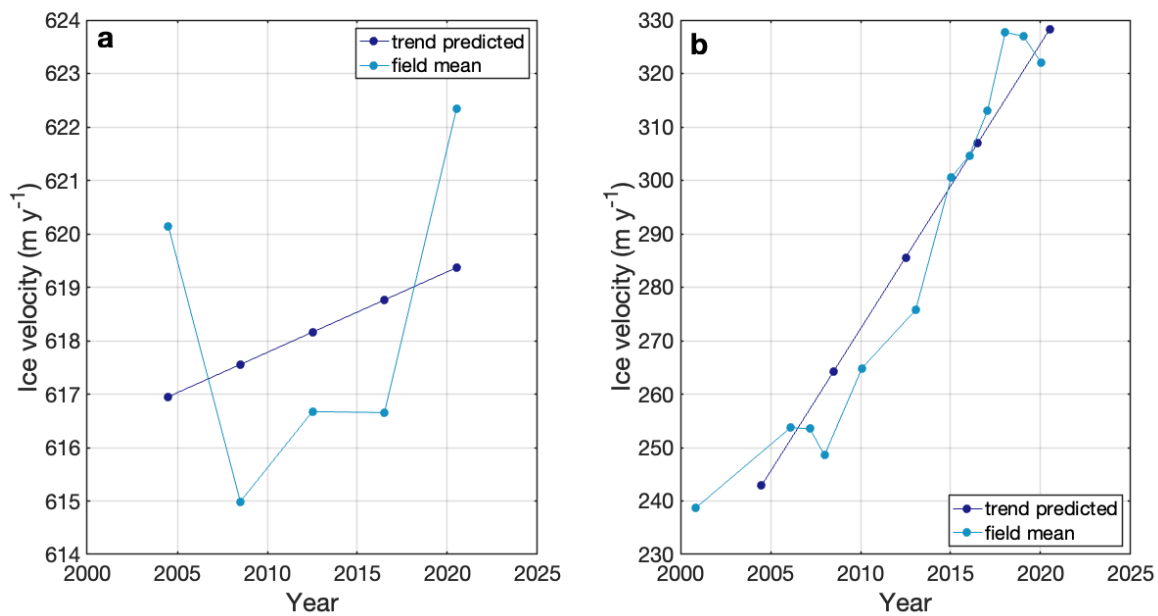


Fig. 8. Mean winter ice velocity and predicted trend based on modeled (a) and observed (b) velocities.

296 of 11.72 Gt yr⁻¹ in 2004 and 11.77 Gt yr⁻¹ in 2020. This implies an increase of 0.05 Gt yr⁻¹ in background
297 basal melt in this region.

298 **Importance of the winter background state**

299 Changes in ice surface elevation alone alter the pattern of basal melting and, over the 2004 to 2020 interval,
300 result in substantial changes in the subglacial winter background state. Our seasonal simulation results
301 (Fig. 5) suggest that the winter background state has a non-negligible influence in determining pressure
302 and velocity magnitudes. The winter background state is determined by ice geometry that has shifted
303 over time on a decadal scale between the eras of ICESat and ICESat-2 observations. It is notable that
304 the seasonal pressure and velocity responses in our seasonal simulations using 2004 and 2020 geometries
305 are offset based on the winter background state when forced with the same transient runoff inputs to the
306 bed, but also exhibit differences in the magnitude of response during the melt season (Fig. 5). While in
307 reality, seasonal forcing evolves over time and also exhibits interannual variability, this modeled exercise
308 allows for isolation of the difference in response due to geometry alone. It is also perhaps unexpected
309 that the ICESat-2 era displays both a decrease in mean modeled effective pressure and mean modeled
310 velocity, as one might expect that a decrease in effective pressure should lead to increased velocity. The
311 key here is that these quantities are mean values over the entire domain; although our simulations produce
312 an increase in effective pressure in the interior, we calculate substantial decreases in effective pressure along
313 the margins, which act to significantly lower the mean value of change in effective pressure. These findings
314 demonstrate the complex impact of changes in surface elevation and the resulting response in ice dynamics,
315 when accounting for the coupled effects of subglacial hydrology.

316 **Limitations**

317 As in any modeling effort, we made informed choices of parameter values and approximations to physics,
318 including choices for ice temperature and rheology, flow law approximation, sliding law, process parameteri-
319 zations, and forcing data. We cannot and do not aim to perfectly reproduce reality with all its complexities,
320 but we do aspire to represent the relevant physical processes in an appropriate way to assess feedbacks and
321 make inferences about realistic behavior of the Greenland Ice Sheet.

322 At least in the early part of our study period (2004-09), the resolution of our elevation-change maps
323 is limited by the track-to-track spacing of the ICESat data, which is up to 20 km in the southern part of

our domain. This means that the elevation-change estimates may not resolve the fine details of surface-elevation change, and may underestimate gradients in elevation change around relatively small topographic features such as outlet glaciers.

We selected our model domain in northwest Greenland based on its significant widespread surface elevation change between 2004 and 2020, representative of the ICESat and ICESat-2 eras (Fig. 2a). Future research should model larger regions of the Greenland Ice Sheet, ideally the entire ice sheet. The work presented here represents advances in coupled subglacial hydrology–ice dynamics modeling using SHAKTI-ISSM on a larger domain than previous applications to single glaciers. Further work should aim to expand these modeling capabilities and establish robust general boundary conditions that can easily be applied to any complicated ice sheet or glacier domain. Moreover, much remains to be explored regarding how best to represent sliding laws and geological friction coefficients while modeling coupled ice velocity and subglacial hydrology.

CONCLUSIONS

In this study, we present large-scale coupled subglacial hydrology and ice dynamics using SHAKTI and ISSM applied to northwest Greenland. We find that changes in ice surface elevation, as observed by satellite laser altimetry from NASA's ICESat and ICESat-2 missions and derived gridded products, yield changes in subglacial hydrology drainage pathways and corresponding ice velocity, along with changes in basal melt rates. We find instances of subglacial flow paths switching between fjords, drawing more water to outlets with enhanced thinning and away from outlets that have retained more of their ice thickness. This reorganization of freshwater discharge holds potential impacts for fjord dynamics, biogeochemistry, and ecology, as well as for frontal ablation rates (including both melt and calving processes). Our simulations demonstrate decreased effective pressure and locations of decreased ice velocity near the margins of the ice sheet, but conversely a modest increase in effective pressure and overall velocity acceleration in the interior. Compared to the observed velocity changes during this period, our coupled model suggests that changes in surface elevation and subglacial hydrology contribute approximately 20% of the total observed velocity change, without accounting for changes in terminus forcing (i.e. changes in terminus position, buttressing, warm water circulation in fjords, etc.). Accompanied by an increase in simulated background basal melt rate, these results suggest feedbacks intensifying mass loss from the Greenland Ice Sheet attributable to changes in ice surface elevation and changes in the subglacial system. The coupled simulations demonstrate

353 the complexity and nuance in accounting for changes in effective pressure due to changes in subglacial
354 hydrology, while highlighting how the ice sheet and its subglacial drainage system respond heterogeneously
355 to changes in surface elevation.

356 ACKNOWLEDGMENTS

357 This study was supported by NASA grants 80NSSC23K1329 and 80NSSC23K0937.

358 DATA AVAILIABILITY

359 We used ISSM version 4.24. ISSM (including SHAKTI) is freely and publicly available for download at
360 <https://github.com/ISSMteam/ISSM>. Model output data and code will be made available in a permanent
361 Zenodo archive for final publication.

362 REFERENCES

- 363 Abdalati W, Zwally HJ, Bindschadler R, Csatho B, Farrell SL, Fricker HA, Harding D, Kwok R, Lefsky M, Markus T,
364 Marshak A, Neumann T, Palm S, Schutz B, Smith B, Spinhirne J and Webb C (2010) The icesat-2 laser altimetry
365 mission. *Proceedings of the IEEE*, **98**(5), 735–751 (doi: 10.1109/JPROC.2009.2034765)
- 366 Andrews LC, Catania GA, Hoffman MJ, Gulley JD, Lüthi MP, Ryser C, Hawley RL and Neumann TA (2014) Direct
367 observations of evolving subglacial drainage beneath the greenland ice sheet. *Nature*, **514**(7520), 80–83
- 368 Badgeley JA, Morlighem M and Seroussi H (2025) Increased sea-level contribution from northwestern greenland for
369 models that reproduce observations. *Proceedings of the National Academy of Sciences*, **122**(25), e2411904122
- 370 Banwell A, Hewitt I, Willis I and Arnold N (2016) Moulin density controls drainage development beneath the
371 greenland ice sheet. *Journal of Geophysical Research: Earth Surface*, **121**(12), 2248–2269
- 372 Budd W, Keage P and Blundy N (1979) Empirical studies of ice sliding. *Journal of Glaciology*, **23**(89), 157–170 (doi:
373 10.3189/S0022143000029804)
- 374 Cowton T, Nienow P, Sole A, Bartholomew I and Mair D (2016) Variability in ice motion at a land-terminating
375 greenlandic outlet glacier: the role of channelized and distributed drainage systems. *Journal of Glaciology*, **62**(233),
376 451–466
- 377 Flowers GE (2015) Modelling water flow under glaciers and ice sheets. *Proceedings of the Royal Society A: Mathe-*
378 *matical, Physical and Engineering Sciences*, **471**(2176), 20140907 (doi: 10.1098/rspa.2014.0907)

- 379 Gelaro R, McCarty W, Suárez MJ, Todling R, Molod A, Takacs L, Randles CA, Darmenov A, Bosilovich MG,
380 Reichle R and others (2017) The modern-era retrospective analysis for research and applications, version 2 (merra-
381 2). *Journal of climate*, **30**(14), 5419–5454
- 382 Hanna E, Navarro FJ, Pattyn F, Domingues CM, Fettweis X, Ivins ER, Nicholls RJ, Ritz C, Smith B, Tulaczyk S
383 and others (2013) Ice-sheet mass balance and climate change. *Nature*, **498**(7452), 51–59
- 384 Jackson RH and Straneo F (2016) Heat, salt, and freshwater budgets for a glacial fjord in greenland. *Journal of*
385 *Physical Oceanography*, **46**(9), 2735–2768
- 386 Joughian I (2023) Measures greenland quarterly ice sheet velocity mosaics from sar and landsat, version 5.
387 *Boulder, Colorado, USA. NASA National Snow and Ice Data Center Distributed Active Archive Center* (doi:
388 10.5067/V5KW64S63OSN)
- 389 Joughin I, Smith BE, Howat IM, Scambos T and Moon T (2010) Greenland flow variability from ice-sheet-wide
390 velocity mapping. *Journal of Glaciology*, **56**(197), 415–430
- 391 Joughin I, Smith B, Howat I and Scambos T (2015) Measures greenland ice sheet velocity map from insar data,
392 version 2 (doi: 10.5067/OC7B04ZM9G6Q)
- 393 Joughin I, Smith BE and Howat I (2018) Greenland ice mapping project: ice flow velocity variation at sub-monthly
394 to decadal timescales. *The Cryosphere*, **12**(7), 2211–2227
- 395 Karlsson NB, Solgaard AM, Mankoff KD, Gillet-Chaulet F, MacGregor JA, Box JE, Citterio M, Colgan WT, Larsen
396 SH, Kjeldsen KK and others (2021) A first constraint on basal melt-water production of the greenland ice sheet.
397 *Nature Communications*, **12**(1), 1–10
- 398 Larour E, Seroussi H, Morlighem M and Rignot E (2012) Continental scale, high order, high spatial resolution, ice
399 sheet modeling using the ice sheet system model (issm). *Journal of Geophysical Research: Earth Surface*, **117**(F1)
400 (doi: 10.1029/2011JF002140)
- 401 MacAyeal DR (1989) Large-scale ice flow over a viscous basal sediment: Theory and application to ice stream B,
402 Antarctica. *Journal of Geophysical Research: Solid Earth*, **94**(B4), 4071–4087 (doi: 10.1029/JB094iB04p04071)
- 403 MacGregor JA, Boisvert LN, Medley B, Petty AA, Harbeck JP, Bell RE, Blair JB, Blanchard-Wrigglesworth E,
404 Buckley EM, Christoffersen MS, Cochran JR, Csathó BM, De Marco EL, Dominguez RT, Fahnestock MA, Farrell
405 SL, Gogineni SP, Greenbaum JS, Hansen CM, Hofton MA, Holt JW, Jezek KC, Koenig LS, Kurtz NT, Kwok
406 R, Larsen CF, Leuschen CJ, Locke CD, Manizade SS, Martin S, Neumann TA, Nowicki SM, Paden JD, Richter-
407 Menge JA, Rignot EJ, Rodríguez-Morales F, Siegfried MR, Smith BE, Sonntag JG, Studinger M, Tinto KJ, Truffer
408 M, Wagner TP, Woods JE, Young DA and Yungel JK (2021) The scientific legacy of nasa's operation icebridge.

- 409 *Reviews of Geophysics*, **59**(2), e2020RG000712 (doi: <https://doi.org/10.1029/2020RG000712>), e2020RG000712
410 2020RG000712
- 411 Mankoff KD, Solgaard A, Colgan W, Ahlstrøm AP, Khan SA and Fausto RS (2020) Greenland ice sheet solid ice
412 discharge from 1986 through march 2020. *Earth System Science Data*, **12**(2), 1367–1383 (doi: [10.5194/essd-12-](https://doi.org/10.5194/essd-12-1367-2020)
413 [1367-2020](https://doi.org/10.5194/essd-12-1367-2020))
- 414 Markus T, Neumann T, Martino A, Abdalati W, Brunt K, Csatho B, Farrell S, Fricker H, Gardner A, Harding D,
415 Jasinski M, Kwok R, Magruder L, Lubin D, Luthcke S, Morison J, Nelson R, Neuenschwander A, Palm S, Popescu
416 S, Shum C, Schutz BE, Smith B, Yang Y and Zwally J (2017) The ice, cloud, and land elevation satellite-2 (icesat-
417 2): Science requirements, concept, and implementation. *Remote Sensing of Environment*, **190**, 260–273, ISSN
418 0034-4257 (doi: <https://doi.org/10.1016/j.rse.2016.12.029>)
- 419 Meierbachtol T, Harper J and Humphrey N (2013) Basal drainage system response to increasing surface melt on the
420 greenland ice sheet. *Science*, **341**(6147), 777–779
- 421 Meyer CR and Hewitt IJ (2017) A continuum model for meltwater flow through compacting snow. *Cryosphere*, **11**(6),
422 2799–2813 (doi: [10.5194/tc-11-2799-2017](https://doi.org/10.5194/tc-11-2799-2017))
- 423 Morlighem M and others (2021) Icebridge bedmachine greenland, version 4 [data set]. *NASA National Snow and Ice*
424 *Data Center Distributed Active Archive Center* (doi: [10.5067/VLJ5YXKCNGXO](https://doi.org/10.5067/VLJ5YXKCNGXO))
- 425 Mouginot J, Rignot E, Bjørk AA, Van den Broeke M, Millan R, Morlighem M, Noël B, Scheuchl B and Wood M
426 (2019) Forty-six years of Greenland Ice Sheet mass balance from 1972 to 2018. *Proceedings of the National Academy*
427 *of Sciences*, **116**(19), 9239–9244 (doi: [10.1073/pnas.1904242116](https://doi.org/10.1073/pnas.1904242116))
- 428 Rada Giacaman CA and Schoof C (2023) Channelized, distributed, and disconnected: spatial structure and temporal
429 evolution of the subglacial drainage under a valley glacier in the yukon. *The Cryosphere*, **17**(2), 761–787
- 430 Rennermalm ÅK, Hock R, Covi F, Xiao J, Corti G, Kingslake J, Leidman SZ, Miège C, Macferrin M, Machguth H
431 and others (2022) Shallow firn cores 1989–2019 in southwest greenland’s percolation zone reveal decreasing density
432 and ice layer thickness after 2012. *Journal of Glaciology*, **68**(269), 431–442
- 433 Schoof C (2005) The effect of cavitation on glacier sliding. *Proceedings of the Royal Society A: Mathematical, Physical*
434 *and Engineering Sciences*, **461**(2055), 609–627
- 435 Schoof C (2010) Ice-sheet acceleration driven by melt supply variability. *Nature*, **468**(7325), 803–806
- 436 Schutz BE, Zwally HJ, Shuman CA, Hancock D and DiMarzio JP (2005) Overview of the icesat mission. *Geophysical*
437 *Research Letters*, **32**(21) (doi: <https://doi.org/10.1029/2005GL024009>)

- 438 Sejr MK, Bruhn A, Dalsgaard T, Juul-Pedersen T, Stedmon CA, Blicher M, Meire L, Mankoff KD and Thyrring J
439 (2022) Glacial meltwater determines the balance between autotrophic and heterotrophic processes in a greenland
440 fjord. *Proceedings of the National Academy of Sciences*, **119**(52), e2207024119
- 441 Shepherd A, Ivins ER, A G, Barletta VR, Bentley MJ, Bettadpur S, Briggs KH, Bromwich DH, Forsberg R, Galin
442 N and others (2012) A reconciled estimate of ice-sheet mass balance. *Science*, **338**(6111), 1183–1189
- 443 Simkins L, Greenwood SL, Munevar Garcia S, Eareckson E, Anderson J and Prothro L (2021) Topographic controls
444 on channelized meltwater in the subglacial environment. *Geophysical Research Letters*, **48**(20), e2021GL094678
- 445 Smith B (2025) *Ice, Cloud, and Land Elevation Satellite-2 (ICESat-2) Project Algorithm Theoretical Basis Document*
446 *(ATBD) for Land-Ice DEM (ATL14) and Land-Ice Height Change (ATL15), Version 5*. NASA Goddard Space
447 Flight Center, Greenbelt, Maryland USA (doi: 10.5067/7INP6DQAWRC2), release 005
- 448 Smith B, Fricker HA, Holschuh N, Gardner AS, Adusumilli S, Brunt KM, Csatho B, Harbeck K, Huth A, Neumann
449 T and others (2019) Land ice height-retrieval algorithm for nasa’s icesat-2 photon-counting laser altimeter. *Remote*
450 *Sensing of Environment*, **233**, 111352
- 451 Smith B, Sutterley TC, Fricker HA, Padman L, Siegfried MR, Black T, Felikson D, Freer BID, Gibbons A, Howard
452 SL, Jelley B, King M, Medley B, Morlighem M, Sadlik C and Sauthoff W (2025) Icesat-2 land ice products
453 resolve greenland and antarctic ice-sheet height changes on seasonal to multiyear time scales (doi: 10.22541/es-
454 soar.175882970.07697715/v1)
- 455 Smith LC, Chu VW, Yang K, Gleason CJ, Pitcher LH, Rennermalm AK, Legleiter CJ, Behar AE, Overstreet
456 BT, Moustafa SE and others (2015) Efficient meltwater drainage through supraglacial streams and rivers on the
457 southwest greenland ice sheet. *Proceedings of the National Academy of Sciences*, **112**(4), 1001–1006
- 458 Sommers A, Rajaram H and Morlighem M (2018) SHAKTI: subglacial hydrology and kinetic, transient interactions
459 v1. 0. *Geoscientific Model Development*, **11**(7), 2955–2974 (doi: 10.5194/gmd-11-2955-2018)
- 460 Sommers A, Meyer C, Morlighem M, Rajaram H, Poinar K, Chu W and Mejia J (2023) Subglacial hydrology modeling
461 predicts high winter water pressure and spatially variable transmissivity at Helheim Glacier, Greenland. *Journal*
462 *of Glaciology*, 1–13 (doi: 10.1017/jog.2023.39)
- 463 Sommers A, Meyer C, Poinar K, Mejia J, Morlighem M, Rajaram H, Warburton K and Chu W (2024) Velocity of
464 greenland’s helheim glacier controlled both by terminus effects and subglacial hydrology with distinct realms of
465 influence. *Geophysical Research Letters*, **51**(15), e2024GL109168
- 466 Straneo F and Cenedese C (2015) The dynamics of greenland’s glacial fjords and their role in climate. *Annual review*
467 *of marine science*, **7**(1), 89–112

- 468 Sundal AV, Shepherd A, Nienow P, Hanna E, Palmer S and Huybrechts P (2011) Melt-induced speed-up of greenland
469 ice sheet offset by efficient subglacial drainage. *Nature*, **469**(7331), 521–524
- 470 Vries AL, van de Berg WJ, Noël B, Meire L and van den Broeke MR (2025) Seasonal and interannual variability in
471 freshwater sources for greenland's fjords. *The Cryosphere*, **19**(9), 3897–3914
- 472 Warburton KL, Meyer CR and Sommers AN (2024) Predicting the onset of subglacial drainage channels. *Journal of*
473 *Geophysical Research: Earth Surface*, **129**(12), e2024JF007758
- 474 Young TJ, Christoffersen P, Bougamont M, Tulaczyk SM, Hubbard B, Mankoff KD, Nicholls KW and Stewart CL
475 (2022) Rapid basal melting of the greenland ice sheet from surface meltwater drainage. *Proceedings of the National*
476 *Academy of Sciences*, **119**(10), e2116036119

For Peer Review

Supplementary Information for "Ice Surface Change Drives Interior Slowdown and Hydrologic Reorganization in Northwest Greenland"

Aleah SOMMERS,¹ Aaron STUBBLEFIELD,^{2,3} Lauren ANDREWS,³ Colin R. MEYER,¹
Benjamin E. SMITH⁴

¹*Thayer School of Engineering, Dartmouth College, Hanover, NH, USA*

²*University of Maryland, College Park, MD, USA*

³*NASA Goddard Space Flight Center, Greenbelt, MD, USA*

⁴*Applied Physics Laboratory, University of Washington, Seattle, WA, USA*

Correspondence: Aleah Sommers <aleah.n.sommers@dartmouth.edu>

Contents of this file:

1. DEM methods
2. Tables S1 to S2
3. Figures S1 to S5

DEM METHODS

Reference DEM estimation

To generate the 2020.5 reference DEM, we adapted the ATL14/15 algorithm in three main ways:

1. ICESat-2 data source: Instead of the ATL11 (along-track slope-corrected height, ?) product, the algorithm used here uses the higher-resolution ATL06 along-track height product (Smith and others, 2019; ?). This allows the ICESat-2 measurements to match the resolution of the ArcticDEM product.
2. ArcticDEM elevation products: To help resolve small-scale topography between ICESat-2 tracks, we include ArcticDEM DEM strips (Porter and others, 2022). These strips provide elevations at 2-m

23 resolution, with near-complete repeat coverage of Greenland 1-2 times per year. We filter and subsample
24 each strip to 32-m resolution, and assign each pixel an estimated uncertainty equal to the RSS (root
25 sum of squares) of a 5-m horizontal geolocation uncertainty times the surface slope, and the RMS
26 difference between pixel's elevation and the elevations of the surrounding pixels in the 2-m input DEM
27 (accumulated using a 32-m Gaussian average). During the surface-fitting process, we solve for an
28 additional set of parameters for each DEM to account for across-track stripe artifacts that result from
29 misalignment of satellite sensor pixels (Shean and others, 2016), and along-track artifacts that sometimes
30 appear in the DEMs, possibly due to imperfections in the sensor geolocation models (similar to Girod
31 and others (2015)). These corrections take the form of one piecewise-linear function with 100-m node
32 spacing in the across-track direction and a second piecewise-linear linear function with 500-m resolution
33 in the along-track direction, where the along-and across-track directions are determined separately for
34 each strip. The coefficients of these functions are determined during the least-track fitting procedure
35 along with the DEM and height-change parameters. We also solve for the uniform per-strip 5-m-RMS
36 vertical elevation bias that has been observed in similar DEMs (Shean and others, 2019).

37 3. Firn-air and surface-mass-balance correction We correct for expected surface-elevation variations driven
38 by snowfall and compaction by subtracting a model that estimates height changes due to accumulation
39 and firn-air content change (Medley and others, 2022). We subtract the sum of the firn-air-content
40 anomaly and the ice-accumulation anomaly from each measured elevation before fitting, then add the ice-
41 accumulation anomaly to the estimated DEM and elevation-change surfaces. These steps are intended
42 to reduce the sampling error that can arise when altimetry data do not evenly sample the seasonal
43 variations in the ice-sheet surface elevation.

44 We apply the fitting algorithm to ICESat-2 and ArcticDEM data spanning 1 January 2019 - 31 De-
45 cember 2023, and solve for a reference DEM for July 1 2020 with a horizontal posting of 50 m and a set of
46 elevation-change surfaces with 0.25-a temporal and 500-m horizontal posting.

47 We perform the calculations on overlapping 18-km tiles, with tile centers separated by 10 km, and
48 mosaick the final products from these tiles using a cosine-taper weighting function in the overlapping
49 regions. We do not use the elevation-change surfaces ($\delta(x, y, t)$) in the current study, but need to include
50 them in the solution to allow data from multiple temporal epochs to contribute to the DEM surface. The
51 result of this procedure is a nearly seamless map of Greenland elevations that includes data that resolve
52 fine-scale surface features almost everywhere on the ice sheet. There are a few regions in south-central

53 Greenland where high-quality ArcticDEM data were not available during our study period; in these areas,
 54 we marked the pixels directly sampled by ICESat-2 (with 200-m tolerance) as valid, and marked the
 55 unconstrained pixels as invalid.

56 Decadal elevation-change estimates

57 To estimate elevation surfaces for 2004, 2008, 2012, and 2016, we apply the surface-fitting algorithm to the
 58 differences between laser-altimetry data spanning 2004-2019 and the reference 2020.5 DEM. We use release
 59 634 ICESat data (Zwally and others, 2014), ATM (Airborne Topographic Mapping system) ICESat data
 60 (Studinger, 2014), and LVIS (Laser Vegetation and Ice measurement System) geolocated surface elevation
 61 product (Blair and Hofton, 2019). The scanning laser altimetry datasets provide data over a swath beneath
 62 the aircraft, and we have found that in some cases small errors in the instrument orientation can produce
 63 artificial tilts in the data which appear in the gridded product as gradients in elevation change. We avoid
 64 this effect by using only a narrow swath of data beneath the instrument. For the ATM data, which reduces
 65 the instrument’s point cloud to a set of planar facets, we select only the near-nadir facet. For LVIS, we
 66 select only the elevation measurements that fell within 50 m of the center of the swath. We convert each
 67 product to the ITRF2014 reference system, relative to the WGS84 ellipsoid, and because our goal is to
 68 create a time-varying surface-elevation estimate for the ice sheet (rather than mass change) we do not
 69 correct for the effects of glacial isostatic adjustment or elastic rebound.

We fit a time series of elevation changes to the subsampled pre-ICESat-2 elevation measurements by
 subtracting 2020.5 DEM from each measurement, then fitting the elevation residuals with a smoothly
 varying surface, on a 500-m horizontal, 1-yr temporal grid:

$$\delta_{pre} = fmin_{\delta_{pre}} \left(\sum_{data} \left(\frac{\delta_{pre} - (z_i - z_{DEM} - b_i - \delta_{SMB,i} - \delta_{FAC,i})}{\sigma_i} \right)^2 + W_{xxt} \int \nabla^2 \delta_{pre} dAdt + \sum_{biases} \left(\frac{b_j}{E(b_j)} \right)^2 \right)$$

70 Here W_{xxt} is a weighting function that describes the importance of model smoothness in the solution
 71 relative to data misfit, b_j represents the biases for each dataset, and $E(b_j)$ is the expected RMS bias for
 72 the dataset; we assume that each dataset has a unique bias value for each day, with an expected RMS
 73 variability of 0.03 m. Solving for uncertain bias values in this way lets us take into account the effects of
 74 correlated errors in the data. We solve for the decadal elevation change on overlapping 40-km tiles, whose
 75 centers are spaced 10 km apart, then mosaic these tiles using a raised-cosine weighting function.

76 **Constructing the elevation time series**

We derive elevations for the DEMs by adding the SMB anomaly to the sum of the DEM and the height-change maps:

$$z(x, y, t) = z_{2020.5}(x, y) + \delta_{pre}x, y, t + \delta_{SMB}x, y, t$$

77 This estimate essentially copies the details of the surface topography in the 2019 DEM to the previous
78 years, using the coarser-resolution elevation-change maps derived from IceBridge and ICESat to constrain
79 the larger-scale changes in ice-sheet topography driven by patterns of ice-sheet mass imbalance.

Table 1. Constants and parameter values used in this study

Symbol	Value	Units	Description
A	3.5×10^{-25}	$\text{Pa}^{-3} \text{ s}^{-1}$	Flow law parameter (for ice at -10°C)
C	Spatially varying	$\text{s}^{1/2} \text{ m}^{-1/2}$	Drag coefficient used in basal stress calculation
G	Spatially varying 0.04-0.06	W m^{-2}	Geothermal flux (Shapiro and Ritzwoller, 2004)
g	9.81	m s^{-2}	Gravitational acceleration
H	Varying	m	Ice thickness
L	3.34×10^5	J kg^{-1}	Latent heat of fusion of water
n	3	Dimensionless	Flow law exponent
z_b	Varying	m	Bed elevation with respect to sea level
ν	1.787×10^{-6}	$\text{m}^2 \text{ s}^{-1}$	Kinematic viscosity of water
ω	0.001	Dimensionless	Parameter controlling nonlinear laminar/turbulent transition
ρ_i	917	kg m^{-3}	Bulk density of ice
ρ_w	1000	kg m^{-3}	Bulk density of water

Table 2. Velocity observations used for comparison to modeled velocities

File name	Date range	Midpoint date	Reference	Notes
greenland_vel_mosaic500_2000_2001_vv_v02.1.tif	3 September 2000 to 24 January 2001	13 November 2000	Joughin et al. (2015)	--
greenland_vel_mosaic500_2005_2006_vv_v02.1.tif	13 December 2005 to 20 April 2006	15 February 2006	Joughin et al. (2015)	--
greenland_vel_mosaic500_2006_2007_vv_v02.1.tif	18 December 2006 to 6 June 2007	13 March 2007	Joughin et al. (2015)	--
greenland_vel_mosaic500_2007_2008_vv_v02.1.tif	7 September 2007 to 23 April 2008	30 December 2007	Joughin et al. (2015)	--
greenland_vel_mosaic500_2008_2009_vv_v02.1.tif	15 September 2008 to 16 June 2009	30 January 2009	Joughin et al. (2015)	Excluded due to limited data extent.
greenland_vel_mosaic500_2009_2010_vv_v02.1.tif	2 September 2009 to 7 May 2010	30 January 2010	Joughin et al. (2015)	--
greenland_vel_mosaic500_2012_2013_vv_v02.1.tif	10 November 2012 to 5 April 2013	22 January 2013	Joughin et al. (2015)	--
greenland_vel_mosaic500_2014_2015_vv_v02.1.tif	1 September 2014 to 31 May 2015	15 January 2015	Joughin et al. (2015)	--
greenland_vel_mosaic500_2015_2016_vv_v02.1.tif	1 September 2015 to 31 May 2016	15 January 2016	Joughin et al. (2015)	--
greenland_vel_mosaic500_2016_2017_vv_v02.1.tif	1 September 2016 to 31 May 2017	15 January 2017	Joughin et al. (2015)	--
greenland_vel_mosaic500_2017_2018_vv_v02.1.tif	1 September 2017 to 31 May 2018	15 January 2018	Joughin et al. (2015)	--
GL_vel_mosaic_Quarterly_01Dec18_28Feb19_vv_v05.0.tif	1 December 2018 to 28 February 2019	15 January 2019	Joughin et al. (2023)	Regrided to 500m.
GL_vel_mosaic_Quarterly_01Dec19_29Feb20_vv_v05.0.tif	1 December 2019 to 29 February 2020	15 January 2020	Joughin et al. (2023)	Regrided to 500m.

80 **SUPPLEMENTAL FIGURES**

81 Incremental changes between 2004-2008, 2008-2012, 2012-2016, 2016-2020.

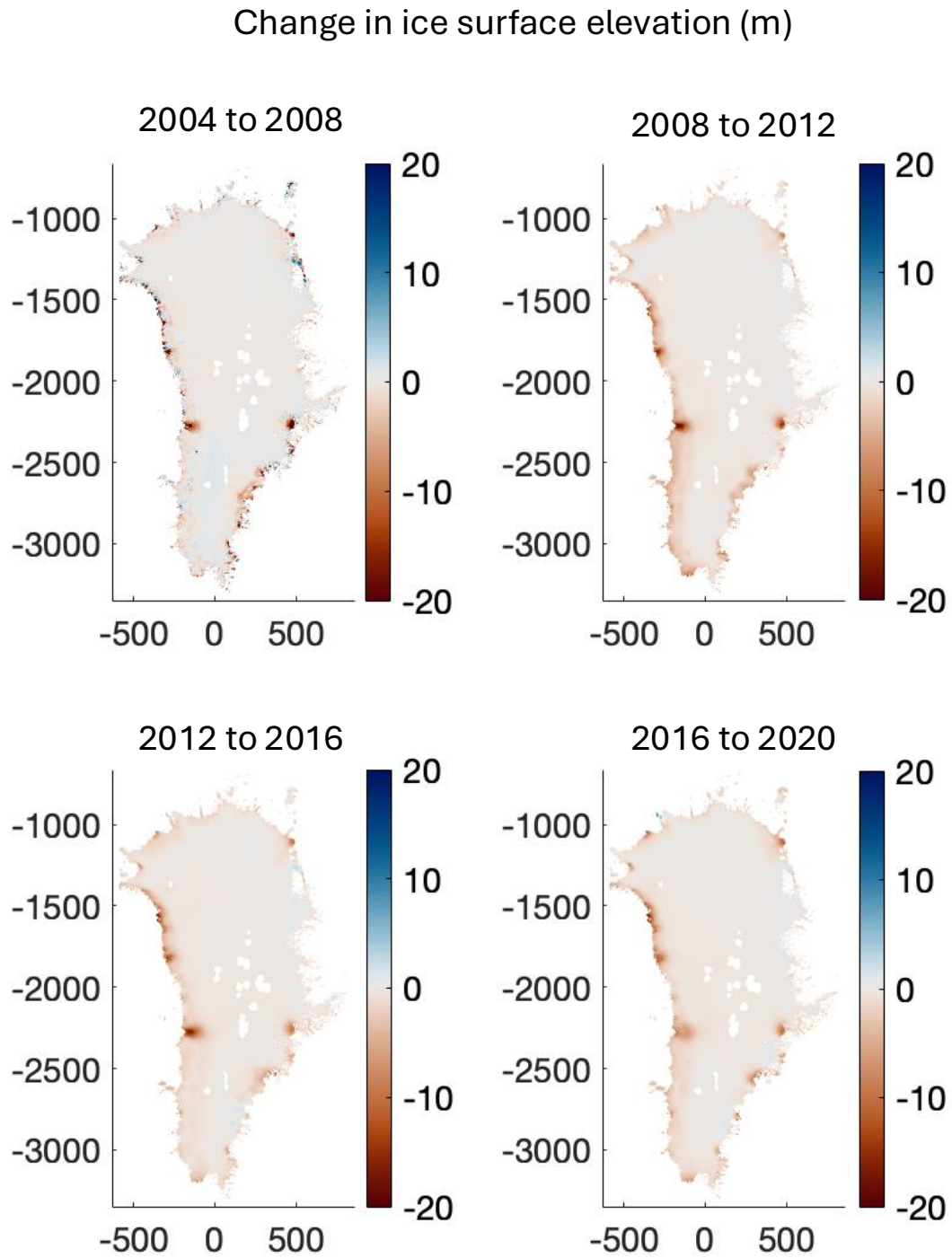


Fig. 1. Change in ice surface elevation of the Greenland Ice Sheet during incremental 4-year periods.

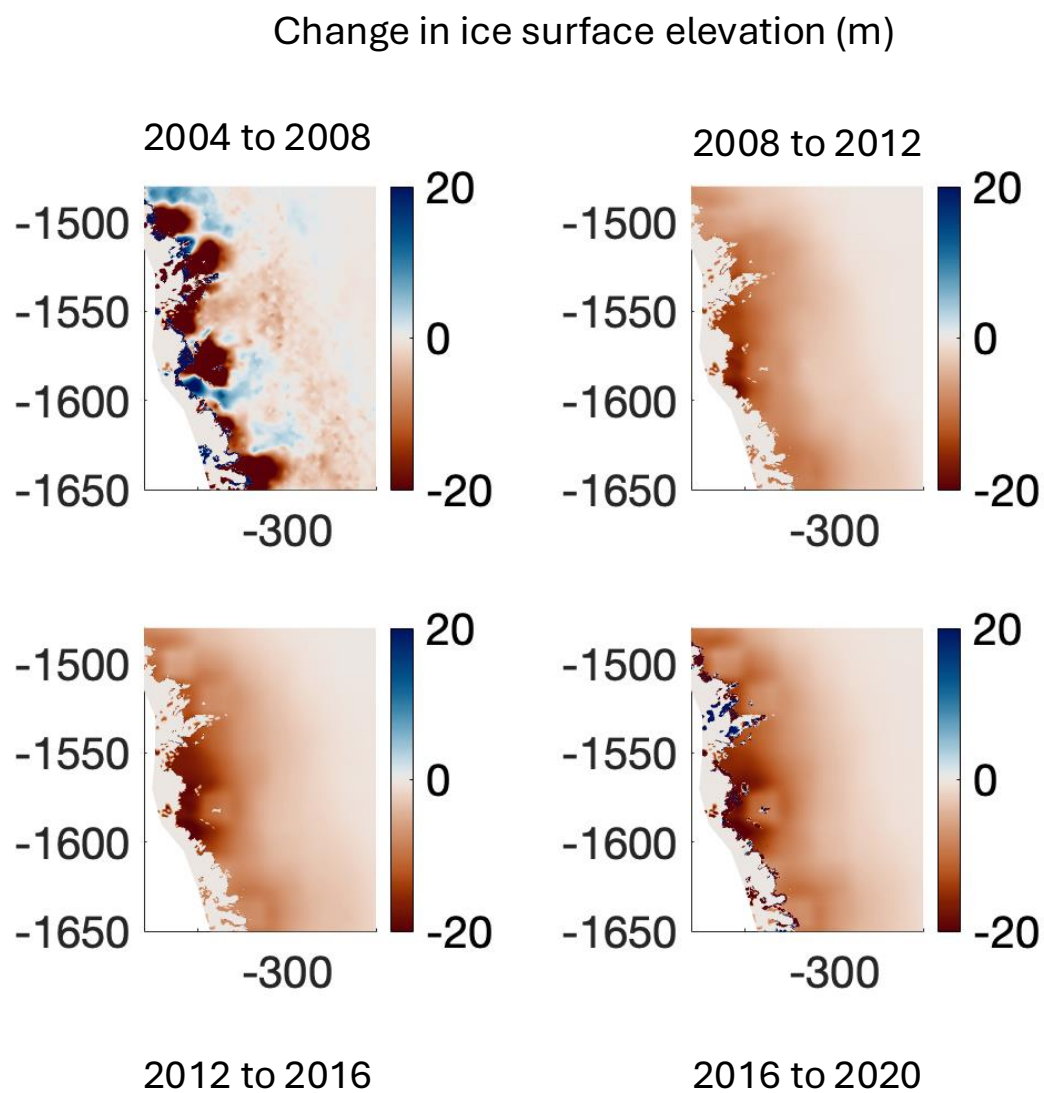


Fig. 2. Change in ice surface elevation in northwest Greenland during incremental 4-year periods.

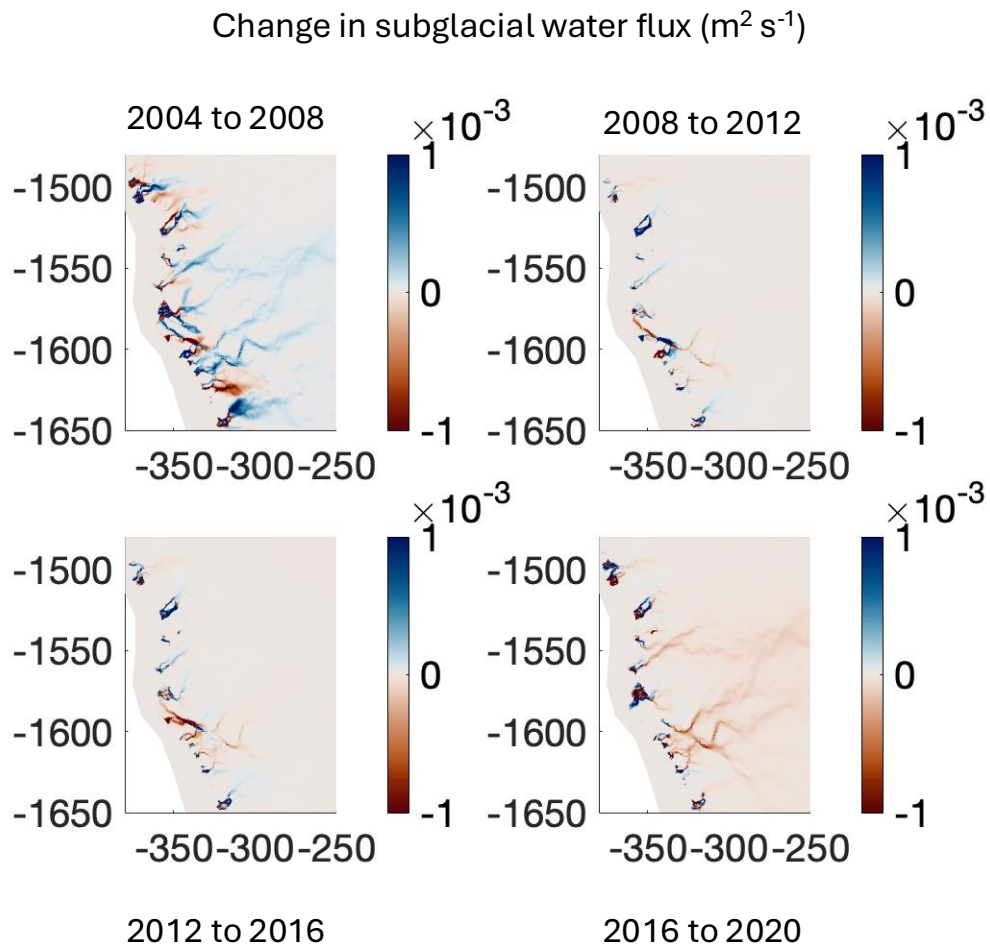


Fig. 3. Change in modeled winter subglacial water flux during incremental 4-year periods.

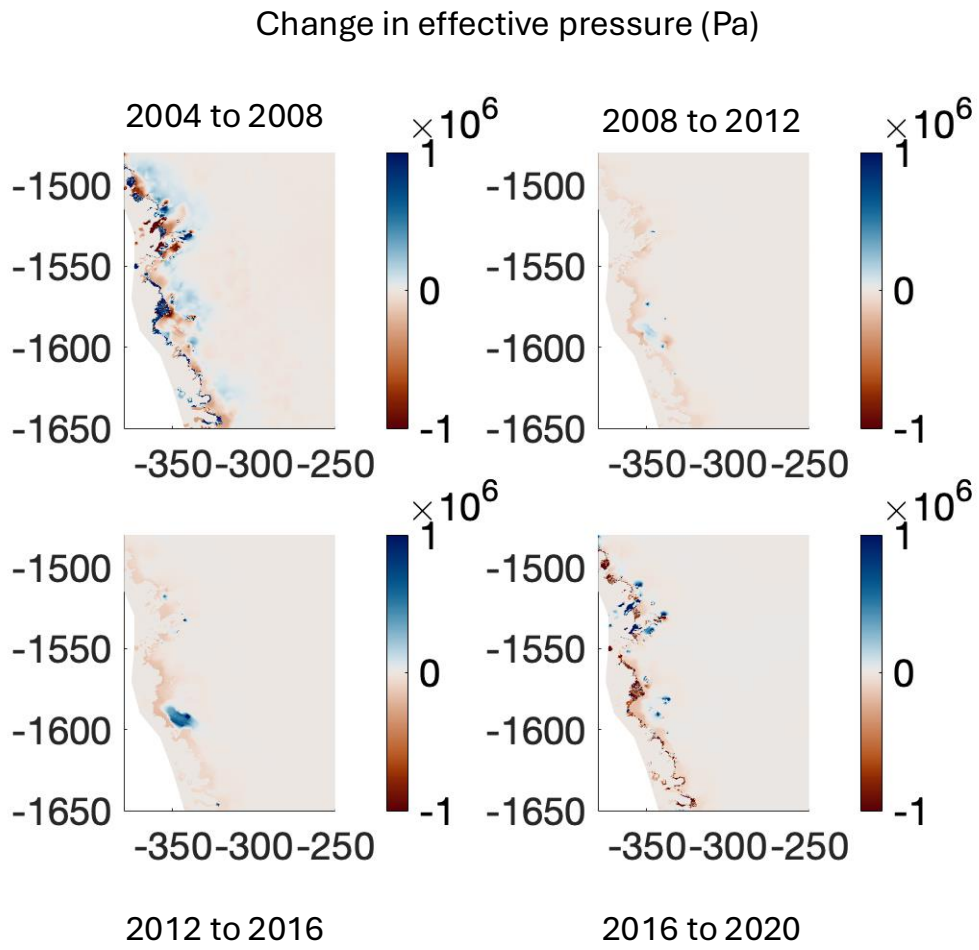


Fig. 4. Change in modeled winter effective pressure during incremental 4-year periods.

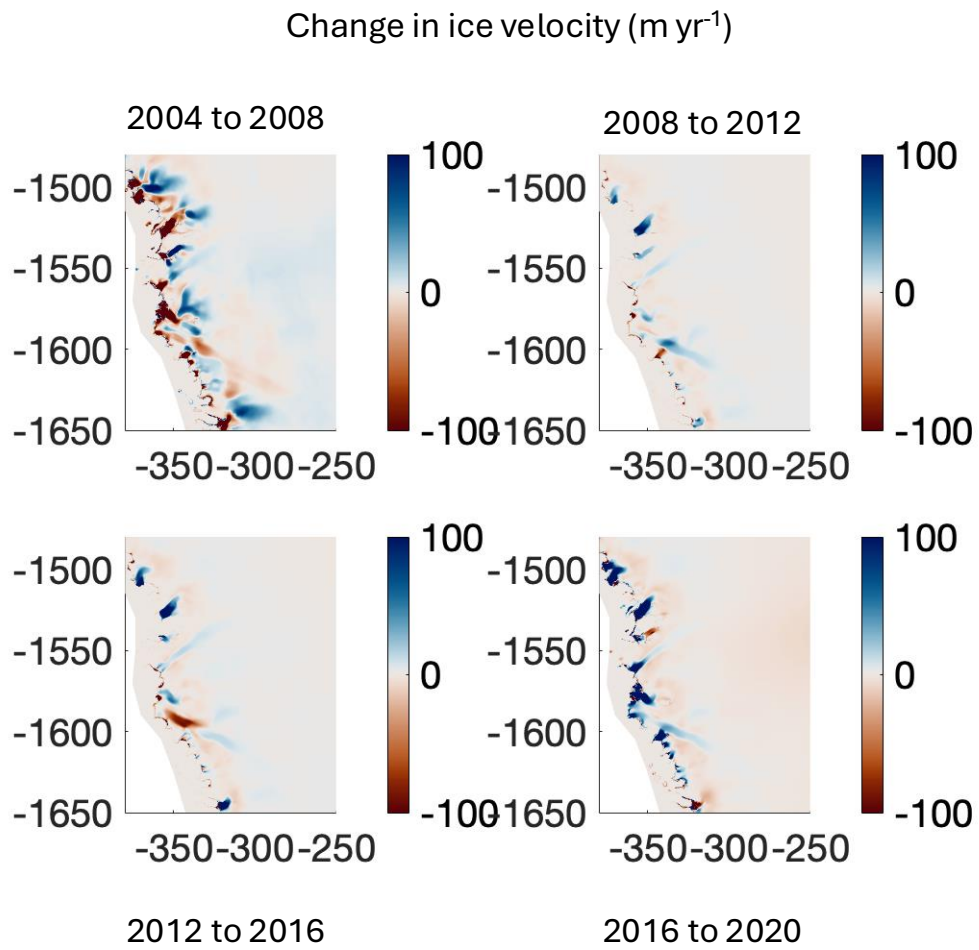


Fig. 5. Change in modeled winter ice velocity during incremental 4-year periods.

82 **REFERENCES**

- 83 Blair J and Hofton M (2019) Icebridge lvis l2 geolocated surface elevation product, version 2 (doi:
84 10.5067/E9E9QSRNLYTK)
- 85 Girod L, Nuth C and Kääb A (2015) Improvement of dem generation from aster images using satellite jitter estimation
86 and open source implementation. *The International Archives of the Photogrammetry, Remote Sensing and Spatial*
87 *Information Sciences*, **XL-1/W5**, 249–253 (doi: 10.5194/isprsarchives-XL-1-W5-249-2015)
- 88 Medley B, Neumann TA, Zwally HJ, Smith BE and Stevens CM (2022) Simulations of firn processes over the
89 greenland and antarctic ice sheets: 1980–2021. *The Cryosphere*, **16**(10), 3971–4011 (doi: 10.5194/tc-16-3971-2022)
- 90 Porter C, Howat I, Noh MJ, Husby E, Khuvis S, Danish E, Tomko K, Gardiner J, Negrete A, Yadav B, Klassen J,
91 Kelleher C, Cloutier M, Bakker J, Enos J, Arnold G, Bauer G and Morin P (2022) ArcticDEM - Strips, Version
92 4.1 (doi: 10.7910/DVN/C98DVS)
- 93 Shapiro NM and Ritzwoller MH (2004) Inferring surface heat flux distributions guided by a global seismic model:
94 particular application to antarctica. *Earth and Planetary Science Letters*, **223**(1-2), 213–224
- 95 Shean DE, Alexandrov O, Moratto ZM, Smith BE, Joughin IR, Porter C and Morin P (2016) An automated, open-
96 source pipeline for mass production of digital elevation models (dems) from very-high-resolution commercial stereo
97 satellite imagery. *ISPRS Journal of Photogrammetry and Remote Sensing*, **116**, 101–117
- 98 Shean DE, Joughin IR, Dutrieux P, Smith BE and Berthier E (2019) Ice shelf basal melt rates from a high-resolution
99 digital elevation model (dem) record for pine island glacier, antarctica. *The Cryosphere*, **13**(10), 2633–2656 (doi:
100 10.5194/tc-13-2633-2019)
- 101 Smith B, Fricker HA, Holschuh N, Gardner AS, Adusumilli S, Brunt KM, Csatho B, Harbeck K, Huth A, Neumann
102 T and others (2019) Land ice height-retrieval algorithm for nasa’s icesat-2 photon-counting laser altimeter. *Remote*
103 *Sensing of Environment*, **233**, 111352
- 104 Studinger M (2014) Icebridge atm l2 icesn elevation, slope, and roughness, version 2 (doi:
105 10.5067/CPRXXK3F39RV)
- 106 Zwally H, Schutz R, Dimarzio J and Hancock D (2014) Glas/icesat l1b global elevation data (hdf5), version 34 (doi:
107 10.5067/ICESAT/GLAS/DATA109)